Ceramics International xxx (xxxx) 1–7

Contents lists available at ScienceDirect

Ceramics International

journal homepage: www.elsevier.com/locate/ceramint

High-quality BeO films fabricated using discrete feeding plasma-enhanced atomic layer deposition

Jonghyun Bae [a, b], Juyoung Chae [a, b], Yoonseo Jang [a, b], Dohwan Jung [a, b], Sangoh Han [a, b], Prakash R. Sultane [c], W. Bielawski [c, d], Jungwoo Oh [a, b, *]

[a] School of Integrated Technology, Yonsei University, Incheon, 21983, Republic of Korea
[b] BK21 Graduate Program in Intelligent Semiconductor Technology, Yonsei University, Incheon, 21983, Republic of Korea
[c] Center for Multidimensional Carbon Materials (CMCM), Institute for Basic Science IBS, Ulsan, 44919, Republic of Korea
[d] Department of Chemistry, Ulsan National Institute of Science and Technology UNIST, Ulsan, 44919, Republic of Korea

ARTICLE INFO

Handling Editor: Dr P. Vincenzini

Keywords:
Beryllium oxide
Discrete feeding method
Plasma-enhanced atomic layer deposition
Gate dielectric
Low impurity

ABSTRACT

In this study, we fabricated high-quality beryllium oxide (BeO) films using discrete-feeding plasma-enhanced atomic layer deposition (DF-PEALD). BeO has exceptionally high thermal conductivity (330 W/m-K), a large bandgap energy, and a high dielectric constant, making it an optimal dielectric that can solve the thermal problems caused by the miniaturization of transistors. In atomic layer deposition (ALD), the physically adsorbed precursors and byproducts present during precursor injection act as a barrier to the full saturation of the substrate surface. The discrete feeding method (DFM) is a process that divides the precursor feeding and purge steps into several individual units without changing the overall process. This mitigates the effects of in-process screening and suppresses the formation of interfacial layers and carbon impurities. The grain size of the BeO fabricated using DF-PEALD was found to be 31.3 % higher than that of BeO fabricated using plasma-enhanced atomic layer deposition (PEALD) without the DFM, and its density (3.01 g/cm^3) more closely matched that of the bulk. The dielectric constant of the BeO films fabricated using DF-PEALD was 8.8, the bandgap energy was 8.1 eV, and the leakage current density was 1.21 × 10^{-9} A/cm^2 at −1 MV/cm.

1. Introduction

Three-dimensional (3D) structures such as fin field-effect transistors (FinFETs) and gate-all-around (GAA) transistors have been developed to address the limitations of conventional planar transistors, especially in terms of their scaling and performance. These advanced architectures have become commercially available, improving the overall efficiency and functionality of complementary metal-oxide-semiconductor (CMOS) devices [1–3]. However, 3D structures are more vulnerable to self-heating because of the low thermal conductivity of the dielectric surrounding the channel, which can increase the temperature and affect the performance and reliability of the device [4–6]. Additionally, high-k materials such as HfO_2 and ZrO_2, used as gate dielectrics in 3D structures because of their attractive electrical properties, have extremely low thermal conductivities, exacerbating these thermal problems. For instance, it was demonstrated that the utilization of Al_2O_3, which exhibits relatively high thermal conductivity (29.0 W/m-K), in GAA not only resulted in a 49 % reduction in thermal resistance in comparison to HfO_2 (0.5 W/m-K), but also led to an improvement in the On-Off ratio by 29.6 % [7,8]. One potential method for addressing this issue is to use a material with optimal electrical properties and high thermal conductivity as the gate dielectric [9,10].

Beryllium oxide (BeO) with a wurtzite structure exhibits a high thermal conductivity of 330 W/m-K at 300 K [11], along with excellent thermal stability [12]. In addition to its unique properties, it has a large bandgap energy of 10.6 eV [13] and a high dielectric constant of 6.9 [14]. Moreover, computational simulations have revealed that BeO with a cubic structure can achieve a dielectric constant of ~275 while maintaining a bandgap energy of 10.1 eV [15]. This makes BeO an appropriate material for mitigating unwanted leakage currents while addressing thermal issues in nanodevices.

Atomic layer deposition (ALD), based on a self-limiting reaction, is suitable for depositing high-quality thin films because of its uniformity, precise thickness control, and conformality [16,17]. BeO thin films fabricated using ALD have been proven to have excellent dielectric properties in Si and various wide bandgap semiconductors such as SiC, GaN, and β-Ga_2O_3 [18–20]. BeO has also been deposited via thermal ALD using various reactants such as H_2O and O_3 [21,22]. Recently, plasma-

* Corresponding author. School of Integrated Technology, Yonsei University, Incheon, 21983, Republic of Korea.
E-mail address: jungwoo.oh@yonsei.ac.kr (J. Oh).

https://doi.org/10.1016/j.ceramint.2025.04.001
Received 2 September 2024; Received in revised form 4 March 2025; Accepted 1 April 2025
0272-8842/

enhanced ALD (PEALD) has been used for the low-temperature growth of BeO, which had better dielectric properties than that fabricated using Thermal ALD (ThALD) [23,24]. However, there is still a lack of systematic research on the ALD of BeO, including methods to control the surface reaction, compared with other materials [25,26]. This may hinder the commercialization of BeO thin films.

The precursor reacts uniformly across the entire surface in an ideal ALD reaction. However, during the actual ALD process, fully saturated reactions do not occur because of steric hindrance and the "screening effect," which was the focus of this study [27]. When excess precursor enters the chamber during the process, a screening effect occurs, which results in both chemical and physical adsorption. The presence of the physically adsorbed precursor hinders the reaction of active sites and reduces the film density [28,29]. The discrete feeding method (DFM) can enhance the quality of thin films while minimizing the consumption of precursors [30–32] by implementing a cut-in purge process without modifying the overall process duration. By repeating the precursor supply and purging processes, physically adsorbed precursors and byproducts can be effectively removed, preventing screening effects and forming high-density thin films [33].

In this study, we systematically investigated the discrete feeding PEALD (DF-PEALD) of BeO films and compared the results with those using conventional PEALD (C-PEALD). The BeO films deposited using the DFM exhibited enhanced crystallinity, which produced superior interface properties, as revealed by a grazing incidence X-ray diffraction (GIXRD) analysis. An X-ray reflectivity (XRR) analysis demonstrated that the density of the BeO film was nearly identical to that of the bulk material, indicating that a denser film was produced. X-ray photoelectron spectroscopy (XPS) results corroborated the observation that the formation of the interfacial layer was not only effectively prevented, as evidenced by the XPS depth profile, but also that pure thin films with almost negligible carbon content were fabricated. The electrical properties were evaluated using metal-oxide-semiconductor (MOS) capacitors, and the superior quality of the BeO thin films fabricated using DF-PEALD was demonstrated.

2. Experiment section

2.1. Sample preparation

P-type Si (100) substrates with a resistivity of ~10 Ω cm were cleaned with acetone, isopropanol (IPA), and deionized water for 5 min each. After cleaning, the Si substrates were immersed in buffered oxide etch (6:1) to remove the native oxide. BeO films were deposited on the Si substrates using an ALD system (Lucida M100-PL, NCD Technology) with Be precursor, diethyl beryllium (DEB, $Be(C_2H_5)_2$) as the precursor [19]. O_2 plasma generated at a radiofrequency of 13.56 MHz served as the reactant in the PEALD process. The O_2 plasma conditions, including a 5 s exposure time, a 50 sccm flow rate, and 100 W power, were previously investigated by our research group for PEALD BeO [34]. The substrate temperature during the PEALD process was maintained at 150 °C, while the precursor temperature was 30 °C. Ar gas maintained a working pressure of 0.25 Torr through a flow rate of 100 sccm to purge any remaining precursor and reactant. Individual saturation curves in terms of pulse time for the C condition and the three DF conditions (DF2, DF3, and DF4), along with a saturation curve for purge time, are provided in the Supporting Information(Fig. S1) to offer a more comprehensive representation of the baseline characteristics for both the C and DF processes.

2.2. Characterization

Ellipsometry (Elli-SE, Ellipso Technology) was used to evaluate the thicknesses of the BeO thin films. GIXRD and XRR analyses were conducted using Rigaku SmartLab systems equipped with an X-ray tube that produced Cu Kα X-rays at 20–60 kV and 60 mA. The compositions of the samples were analyzed via X-ray photoelectron spectroscopy (XPS) using a Thermo Fisher Scientific K-ALPHA system. Al Kα X-rays with an energy of 1486.6 eV were applied with a spot size ranging from 30 to 400 μm and an energy resolution of 0.085 eV. An XPS depth profile analysis was conducted after the sample surface was etched using Ar-ion etching to evaluate the carbon composition.

To fabricate a MOS capacitor, 200 cycles of BeO films were deposited on p-type Si using two different methods: DF-PEALD and C-PEALD. Subsequently, 100 nm of W metal was deposited by DC sputtering after the BeO film growth. A shadow mask with a 150 μm diameter hole pattern was employed for the deposition of the top electrode. The capacitance–voltage (C–V) and current–voltage (J–E) data were analyzed using a power device analyzer/curve tracker (Keysight B1505A and Keithley 4200-SCS) with a preAMP.

3. Results and discussion

Fig. 1(a) illustrates the BeO deposition sequences using DF-PEALD and C-PEALD. To demonstrate the impact of varying the number of divisions in the feed-purge step, the DF-PEALD sequence was modified to divide the precursor feed-purge step into two, three, and four steps without altering the total process time (D2, D3, and D4). As shown in Fig. 1(b), in C-PEALD, the screening effect is caused by physically adsorbed precursors and byproducts, owing to the lack of a purge, which screens the reactive site. In contrast, the DF-PEALD process employs a "cut-in purging" technique to remove residual DEB precursors and byproducts [30] effectively. This technique exposes the active sites on the surface, allowing a subsequent short feeding process to efficiently fill the substrate, resulting in a higher-density BeO film deposition. Moreover, the DFM applied to the PEALD process effectively reduced the oxidation of the exposed substrates, thereby minimizing the formation of an undesirable interfacial layer [31].

The growth per cycle(GPC) of DF-PEALD and C-PEALD were measured using an ellipsometer (Fig. 2(a)). Both processes exhibited a linear increase in thickness because of the self-limiting nature of the surface reaction involved in the ALD process. The GPC was determined to be 1.35 Å per cycle for the C-PEALD process and 1.11–1.29 Å per cycle for the DF-PEALD process, indicating that the GPC decreased as the pulse purge steps became more divided. The effects of the DFM approach on GPC have been reported in the literature, with some studies observing an increase in GPC due to the removal of screening effects, while others report a reduction in GPC associated with the growth of denser films through the removal of unreacted precursors and ligands [28,37]. In this study, the DFM method for BeO thin films resulted in an earlier saturation region and slightly lower GPC compared to C-PEALD. The reduction in the GPC of the BeO layer indicated that it underwent densification owing to the DFM method [35]. The ALD window and refractive index of C-PEALD and DF-PEALD BeO films are shown in Fig. S2.

The DFM method is expected to result in the deposition of denser BeO films than the C-PEALD method, owing to the filling of the screened active sites. XRR analyses were conducted to compare the film densities of the C-PEALD and DF-PEALD films (Fig. 2(b)). The density of BeO was 3.01 g/cm^3 after DF-PEALD (D4), which was higher than that after C-PEALD (2.70 g/cm^3) and close to the density of bulk BeO (3.00–3.01 g/cm^3) [36]. Furthermore, the density increased with the number of divisions, with C-PEALD producing the lowest density and DF-PEALD (D4) producing the highest. This indicated that the precursor engaged with more of the substrate and contained a reduced quantity of impurities, such as carbon [37]. Based on these results, analyses were performed focusing on DF-PEALD (D4) and conventional methods.

The crystal structures of BeO deposited on Si substrates using the DFM and conventional methods were analyzed based on the GIXRD. A

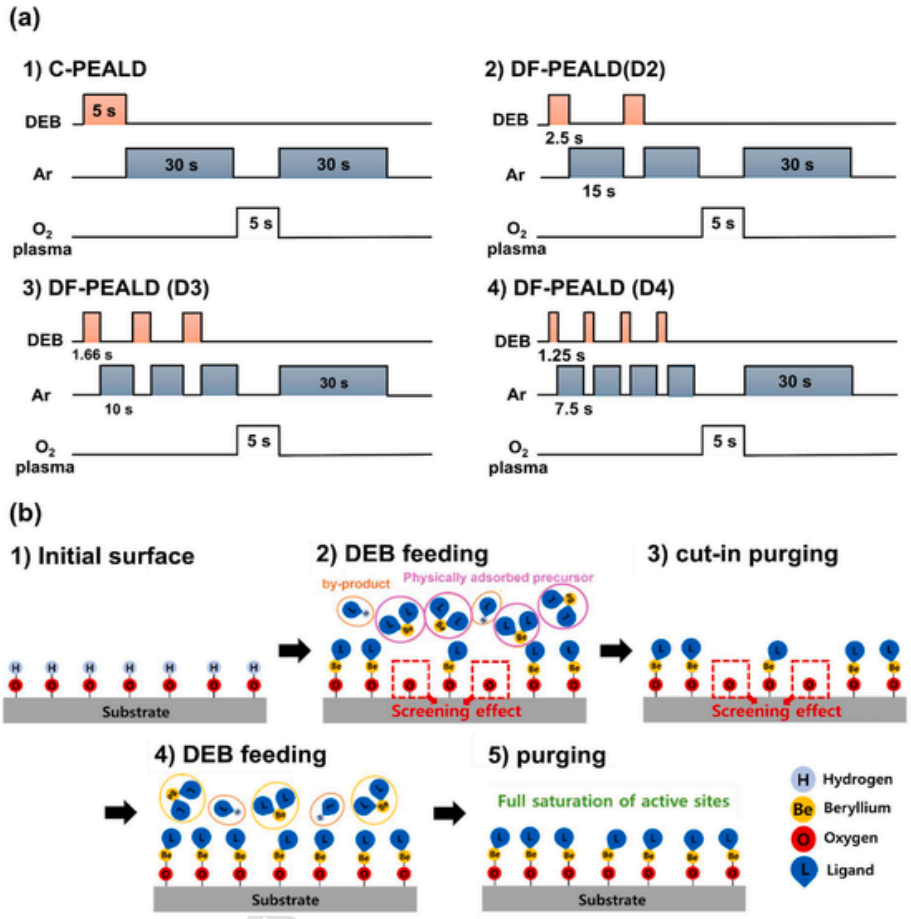

Fig. 1. (a) Process sequences of the C-PEALD and DF-PEALD divided into N steps: D2 (2), D3 (3), and D4 (4). **(b)** Schematic of the mechanism for the PEALD of BeO films with a discrete feeding method. The screening effect was suppressed by the cut-in purging process.

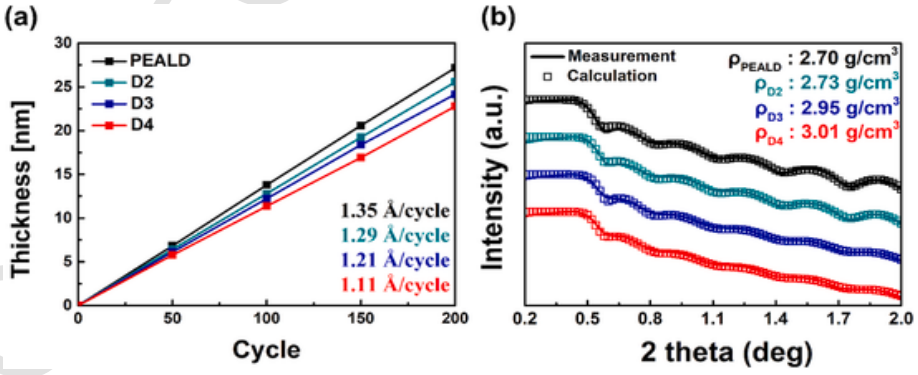

Fig. 2. (a) Comparison of thicknesses of BeO films fabricated using C-PEALD and DF-PEALD with different numbers of cycles. (b) Measured XRR curve and calculated curves of BeO films fabricated using different sequences. The BeO density exhibited an increase in correlation with the intensification of the cut-in purge process.

comparison was made with the ICDD XRD database and reference database [38], and Fig. 3 shows a BeO (002) peak at 41.1° after C-PEALD and 41.17° after DF-PEALD, indicating that wurtzite BeO grew along the c-axis on Si(001) in both processes. To ascertain the degree of crystallinity, the grain size was determined by the full width at half maximum (FWHM) of the GIXRD data. The equation for calculating the average grain size (D_p) of BeO on Si is as follows: $D_p = (0.94 \times \lambda)/(\beta \times \cos\theta)$, where λ, β, and θ represent the line broadening in radians, Bragg angle, and X-ray wavelength [39,40], respectively. The D_p values for the BeO (002) fabricated using DF-PEALD and C-PEALD were approximately 13.85 nm and 10.55 nm, respectively. In this study, the grain size derived from GIXRD analysis represents the out-of-plane crystallite size. While this provides valuable information about the vertical crystallographic structure, it does not necessarily capture the in-plane grain size, which is more directly influenced by nucleation density. Although EBSD (Electron Backscatter Diffraction) could complement XRD

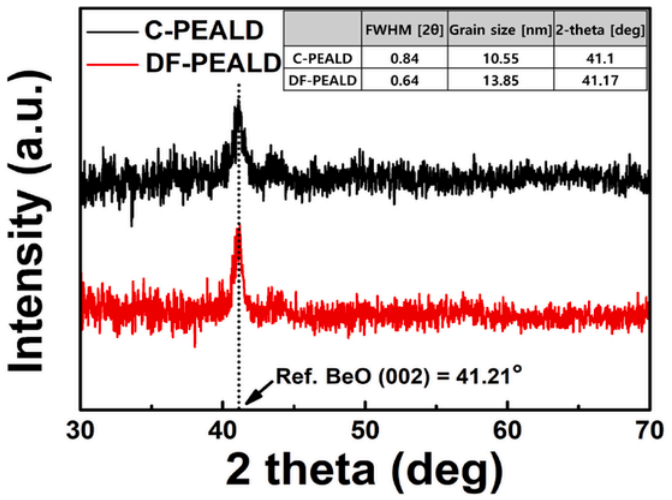

Fig. 3. GIXRD patterns for BeO thin films on Si prepared using C-PEALD and DF-PEALD. The BeO (0 0 2) planes were observed at 41.1°–41.17°, and the grain size of the BeO film was found to increase through the application of the DFM method.

by providing in-plane grain size for a more comprehensive evaluation, it requires a thicker film than that of our ALD-depositied BeO films. Instead, we attemped azimuthal scans to assess in-plane crystallinity (Fig. S4). This results supports the possibility of increased in-plane grain size in BeO-on-Si as well. It can be concluded that the enhanced grain size of the BeO films on Si is expected to improve their electrical properties by reducing the defects associated with dangling bonds [41]. Furthermore, a higher crystallinity for BeO thin films is anticipated to result in enhanced thermal conductivity [42,43].

Fig. 4 shows the chemical binding states of the BeO films, which were analyzed using XPS. The core-level Be 1s and O 1s spectra indicate that the chemical structures of both films were almost identical. However, a significant difference was observed in the Si 2p core-level spectra of the two thin films. In contrast to the DF-PEALD-deposited BeO, a larger peak corresponding to Si-O bonding (SiO_x) was observed at 102.9 eV for the C-PEALD-deposited BeO [44]. The concentration of Si-O bonds was calculated using the XPS Si 2P ratio. The Si-O bonding ratio was 13.25 % when the DFM was used, significantly lower than the 28.5 % obtained by conventional methods. The observed Si-O bonding peak resulted from the interfacial layer [45], thereby demonstrating that the DFM effectively prevented substrate oxidation. Repeated cycles of cut-in purging and subsequent DEB feeding not only remove residual by-products but also ensure efficient filling of the exposed Si substrate. This process significantly reduces the susceptibility of the substrate to oxidation during subsequent steps. Such repeated cycles mitigate oxidation effects over multiple DF cycles, resulting in the observed suppression of the Si-O signal compared to the conventional process. In conclusion, the DFM reduced the screening effect and suppressed the interfacial layer formation.

Fig. 5 compares the elemental compositions of the films based on the XPS depth profiles. The DF-PEALD produced a significantly lower carbon impurities (0.35 %) than the C-PEALD (2.57 %). The BeO film fabricated using DF-PEALD had a remarkably low carbon impurity content, suggesting that impurities such as byproducts were effectively purged during the ALD process. In addition, the XPS depth profile was used to measure the oxidized interfacial layer. The suppression of the native SiO_2 by the DFM, as illustrated in Fig. 4, could be substantiated by the data presented in Fig. 5 [46] .

Notably, the Be concentration increased significantly when the DFM was applied. The O/Be ratio was 0.94 for DF-PEALD compared to 1.03 for C-PEALD. The use of DFM during DEB precursor injection appears to have facilitated the deposition of a denser layer, leading to an increase in Be content relative to O content. A promising direction for future investigations could be the simultaneous application of a discrete reac-

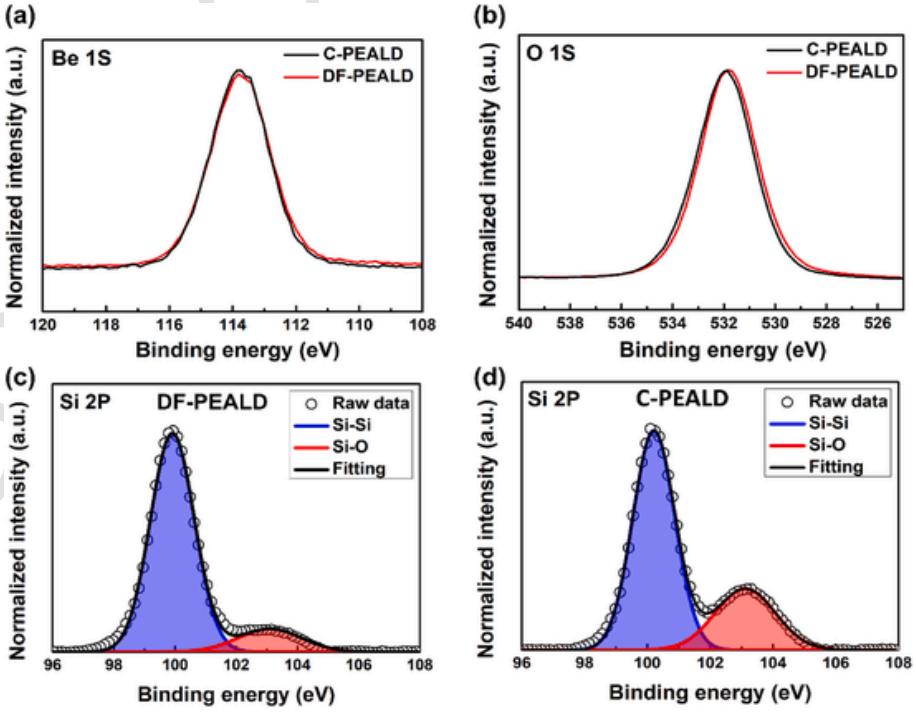

Fig. 4. (a) Be 1s and (b) O1s core level XPS spectra of BeO films grown via C-PEALD and DF-PEALD processes and Si 2p core level XPS spectra of BeO films grown via (c) DF-PEALD and (d) C-PEALD processes.

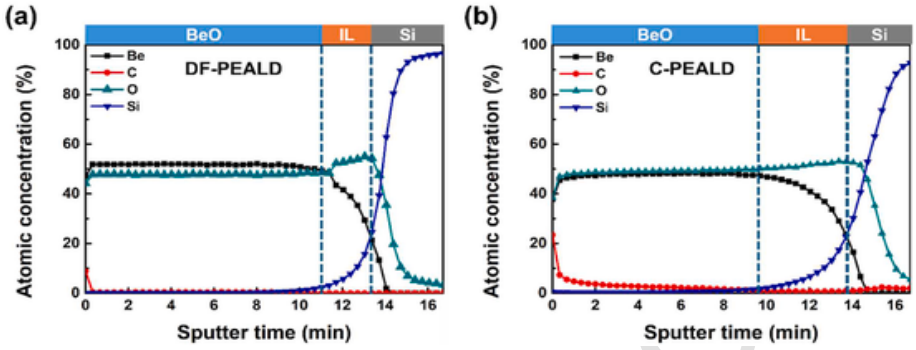

Fig. 5. XPS depth profiles of Be, O, Si, and C after the (a) DF-PEALD and (b) C-PEALD of BeO films. The use of DF-PEALD resulted in notable reductions in the carbon impurities and interlayer compared to C-PEALD.

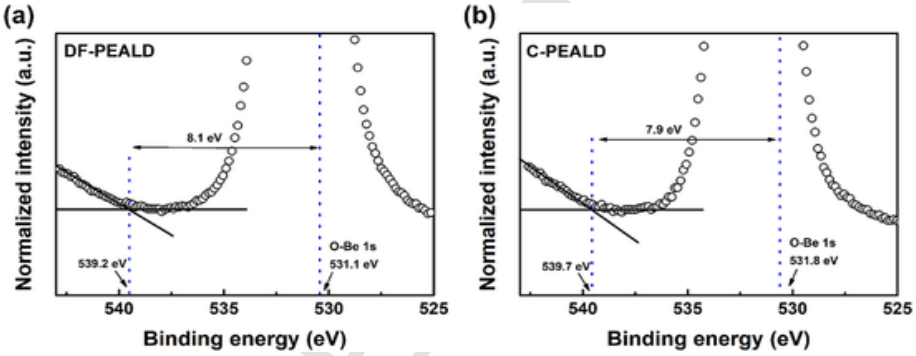

Fig. 6. XPS O1s spectra of BeO films fabricated using the DF-PEALD and C-PEALD techniques. The band gap energies were calculated by subtracting the core level binding energy from the inelastic collision energy.

tant feeding method to enhance the effectiveness of the O_2 plasma exposure step and potentially achieve a more balanced Be:O ratio [47].

The bandgap energy values, as determined from the XPS O1s spectra of the BeO films produced by the DF-PEALD and C-PEALD methods, were calculated by subtracting the inelastic collision energy from the core-level binding energy, following the fitting of a line to the inelastic loss spectra and background level [48]. Bandgap energy values of 8.1 eV and 7.9 eV were measured for DF-PEALD and C-PEALD, comparable to the reference value obtained using the ALD method [21,23].

A comparative analysis of the electrical characteristics of the MOS capacitors fabricated with BeO using DF-PEALD and C-PEALD is presented in Fig. 7. The C–V curves were measured at a frequency of 1 MHz for forward and reverse biases, as shown in Fig. 7(a). The dielectric constant of the BeO film (8.8) fabricated using DF-PEALD was higher than that of the BeO film (7.54) fabricated using C-PEALD. However, the C–V curve of the film fabricated using DF-PEALD exhibited a positive shift, which could be attributed to the relative increase in Be content induced by the DFM, as shown in Fig. 5. This occurred because the higher Be:O ratio influenced charge compensation by reducing the hole concentration, leading to the observed shift. [49]. A comparison of the leakage currents is shown in Fig. 7(b). The film fabricated using DF-PEALD showed a leakage current density of 1.21×10^{-9} A/cm^2 at an electric field of −1 MV/cm, which was less than that of the film fabricated using PEALD (3.7×10^{-8} A/cm^2). The improved electrical properties were attributed to the deposition of dense BeO films with lower impurity concentrations, as well as the suppression of the formation of

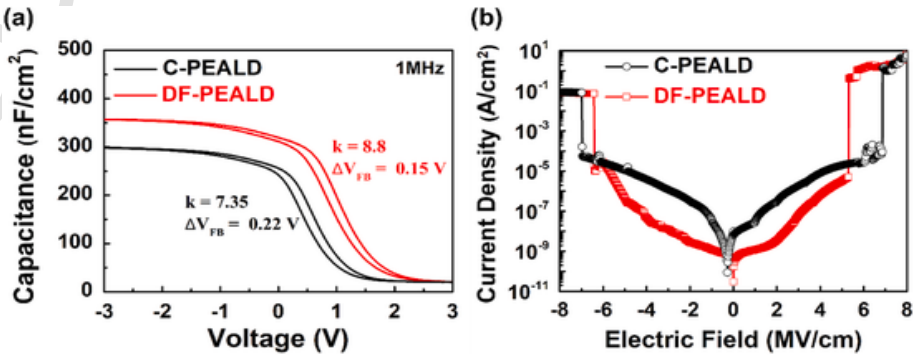

Fig. 7. Electrical characteristics of MOS capacitors: (a) C–V curves measured at 1 MHz with forward and reverse biases and (b) current density–electric field curves.

interfacial layers that cause leakage currents. BeO, with enhanced chemical and electrical properties deposited by the DF-PEALD process, is expected to be used as a dielectric in a variety of advanced devices in the future.

4. Conclusion

In this study, we fabricated PEALD BeO thin films using a discrete feeding method and investigated their physical and chemical qualities. DF-PEALD facilitated the deposition of high-quality thin films by reducing the screening effect during the ALD process while maintaining the total processing time. The density of the BeO film fabricated using DF-PEALD increased to that of bulk BeO, thereby confirming the growth of a high-density film. The BeO films fabricated using DF-PEALD had minimal carbon impurities of 0.35 % and higher crystallinity than those fabricated using C-PEALD. The interfacial layer created during the ALD process was suppressed, improving electrical properties. Following the application of the DFM, the dielectric constant of the BeO film increased to 8.8, accompanied by a reduction in the leakage current. These results indicated that combining the PEALD method with the DFM holds promise for the deposition of high-quality ultrathin BeO films at low temperatures for next-generation three-dimensional transistors.

CRediT authorship contribution statement

Jonghyun Bae: Writing – original draft, Investigation, Formal analysis, Conceptualization. **Juyoung Chae:** Validation, Investigation. **Yoonseo Jang:** Formal analysis, Data curation. **Dohwan Jung:** Validation, Data curation. **Sangoh Han:** Validation. **Prakash R. Sultane:** Validation. **W. Bielawski:** Writing – review & editing, Methodology. **Jungwoo Oh:** Writing – review & editing, Supervision, Formal analysis, Conceptualization.

Declaration of competing interest

The authors declare that they have no known competing financial interests or personal relationships that could have appeared to influence the work reported in this paper.

Acknowledgments

This research was supported by BK21 Fostering Outstanding Universities for Research (FOUR), funded by the Ministry of Education (MOE) of Korea and the National Research Foundation (NRF) of Korea. CWB and PRS acknowledge the IBS for support (IBS-R019-D01).

Appendix A. Supplementary data

Supplementary data to this article can be found online at https://doi.org/10.1016/j.ceramint.2025.04.001.

References

[1] H. Iwai, CMOS scaling toward sub-10 nm regime, in: The 11th IEEE International Symposium on Electron Devices for Microwave and Optoelectronic Applications, 2003. EDMO 2003, IEEE, 2003, pp. 30–34.
[2] B. Yu, L. Chang, S. Ahmed, H. Wang, S. Bell, C.-Y. Yang, C. Tabery, C. Ho, Q. Xiang, T.-J. King, FinFET scaling to 10 nm gate length, in: Digest. International Electron Devices Meeting, 2002, pp. 251–254 IEEE.
[3] N. Loubet, T. Hook, P. Montanini, C.-W. Yeung, S. Kanakasabapathy, M. Guillom, T. Yamashita, J. Zhang, X. Miao, J. Wang, Stacked nanosheet gate-all-around transistor to enable scaling beyond FinFET, in: 2017 Symposium on VLSI Technology, IEEE, 2017, pp. T230–T231.
[4] M.I. Khan, A.R. Buzdar, F. Lin, Self-heating and reliability issues in FinFET and 3D ICs, in: 2014 12th IEEE International Conference on Solid-State and Integrated Circuit Technology, ICSICT), IEEE, 2014, pp. 1–3.
[5] S.J. Kang, J.H. Kim, Y.S. Song, S. Go, S. Kim, Investigation of self-heating effects in vertically stacked GAA MOSFET with wrap-around contact, IEEE Trans. Electron. Dev. 69 (2022) 910–914.
[6] Y.S. Song, J.H. Kim, G. Kim, H.-M. Kim, S. Kim, B.-G. Park, Improvement in self-heating characteristic by incorporating hetero-gate-dielectric in gate-all-around MOSFETs, IEEE J. Electron Devices Soc. 9 (2020) 36–41.
[7] E.P. Gusev, C. Cabral Jr, M. Copel, C. D'emic, M. Gribelyuk, Ultrathin HfO2 films grown on silicon by atomic layer deposition for advanced gate dielectrics applications, Microelectron. Eng. 69 (2003) 145–151.
[8] D. Vanderbilt, X. Zhao, D. Ceresoli, Structural and dielectric properties of crystalline and amorphous ZrO2, Thin Solid Films 486 (2005) 125–128.
[9] Y.S. Song, S. Kim, J.H. Kim, G. Kim, J.-H. Lee, W.Y. Choi, Enhancement of thermal characteristics and on-current in GAA MOSFET by utilizing Al 2 O 3-based Dual-κ spacer structure, IEEE Trans. Electron. Dev. 70 (2022) 343–348.
[10] M. Amani, A.K. Panigrahy, A. Choubey, S.B. Choubey, V.B. Sreenivasulu, D.V. Nair, R. Swain, Design and comparative analysis of FD-SOI FinFET with dual-dielectric spacers for high speed switching applications, Silicon 16 (2024) 1525–1534.
[11] G.A. Slack, S. Austerman, Thermal conductivity of BeO single crystals, J. Appl. Phys. 42 (1971) 4713–4717.
[12] D.W. Johnson, J.H. Yum, T.W. Hudnall, R.M. Mushinski, C.W. Bielawski, J.C. Roberts, W.-E. Wang, S.K. Banerjee, H.R. Harris, Characterization of ALD beryllium oxide as a potential high-k gate dielectric for low-leakage AlGaN/GaN MOSHEMTs, J. Electron. Mater. 43 (2014) 151–154.
[13] D. Roessler, W. Walker, E. Loh, Electronic spectrum of crystalline beryllium oxide, J. Phys. Chem. Solid. 30 (1969) 157–167.
[14] M. Subramanian, R. Shannon, B. Chai, M. Abraham, M. Wintersgill, Dielectric constants of BeO, MgO, and CaO using the two-terminal method, Phys. Chem. Miner. 16 (1989) 741–746.
[15] W.C. Lee, S. Kim, E.S. Larsen, J.-H. Choi, S.-H. Baek, M. Lee, D.-Y. Cho, H.-K. Lee, C.S. Hwang, C.W. Bielawski, Atomic engineering of metastable BeO6 octahedra in a rocksalt framework, Appl. Surf. Sci. 501 (2020) 144280.
[16] S.M. George, Atomic layer deposition: an overview, Chem. Rev. 110 (2010) 111–131.
[17] R.W. Johnson, A. Hultqvist, S.F. Bent, A brief review of atomic layer deposition: from fundamentals to applications, Mater. Today 17 (2014) 236–246.
[18] S.M. Lee, Y. Jang, J. Jung, J.H. Yum, E.S. Larsen, C.W. Bielawski, W. Wang, J.-H. Ryou, H.-S. Kim, H.-Y. Cha, Atomic-layer deposition of crystalline BeO on SiC, Appl. Surf. Sci. 469 (2019) 634–640.
[19] S.M. Lee, J.H. Yum, S. Yoon, E.S. Larsen, W.C. Lee, S.K. Kim, S. Shervin, W. Wang, J.-H. Ryou, C.W. Bielawski, Atomic-layer deposition of single-crystalline BeO epitaxially grown on GaN substrates, ACS Appl. Mater. Interfaces 9 (2017) 41973–41979.
[20] D. Jung, Y. Jang, P.R. Sultane, C.W. Bielawski, J. Oh, Energy band offsets of BeO dielectrics grown via atomic-layer deposition on β-Ga2O3 substrates, J. Alloys Compd. 922 (2022) 166197.
[21] W.C. Lee, C.J. Cho, S. Kim, E.S. Larsen, J.H. Yum, C.W. Bielawski, C.S. Hwang, S.K. Kim, Growth and characterization of BeO thin films grown by atomic layer deposition using H2O and O3 as oxygen sources, J. Phys. Chem. C 121 (2017) 17498–17504.
[22] J. Yum, T. Akyol, M. Lei, D. Ferrer, T.W. Hudnall, M. Downer, C. Bielawski, G. Bersuker, J. Lee, S. Banerjee, A study of highly crystalline novel beryllium oxide film using atomic layer deposition, J. Cryst. Growth 334 (2011) 126–133.
[23] Y. Jang, D. Jung, P.R. Sultane, E.S. Larsen, C.W. Bielawski, J. Oh, Low temperature growth of Beryllium Oxide thin films prepared via plasma enhanced atomic layer deposition, Appl. Surf. Sci. 572 (2022) 151405.
[24] Y. Jang, D. Jung, P.R. Sultane, C.W. Bielawski, J. Oh, Polarization-Induced Two-Dimensional electron gas at BeO/ZnO interface, Appl. Surf. Sci. 600 (2022) 154103.
[25] H.-Y. Shih, W.-H. Lee, W.-C. Kao, Y.-C. Chuang, R.-M. Lin, H.-C. Lin, M. Shiojiri, M.-J. Chen, Low-temperature atomic layer epitaxy of AlN ultrathin films by layer-by-layer, in-situ atomic layer annealing, Sci. Rep. 7 (2017) 39717.
[26] A.J. Mackus, M.J. Merkx, W.M. Kessels, From the bottom-up: toward area-selective atomic layer deposition with high selectivity, Chem. Mater. 31 (2018) 2–12.
[27] T. Muneshwar, K. Cadien, AxBAxB… pulsed atomic layer deposition: numerical growth model and experiments, J. Appl. Phys. 119 (2016).
[28] J.C. Park, C.I. Choi, S.-G. Lee, S.J. Yoo, J.-H. Lee, J.H. Jang, W.-H. Kim, J.-H. Ahn, J.H. Kim, T.J. Park, Advanced atomic layer deposition: metal oxide thin film growth using the discrete feeding method, J. Mater. Chem. C 11 (2023) 1298–1303.
[29] J.W. Han, H.S. Jin, Y.J. Kim, J.S. Heo, W.-H. Kim, J.-H. Ahn, J.H. Kim, T.J. Park, Advanced atomic layer deposition: ultrathin and continuous metal thin film growth and work function control using the discrete feeding method, Nano Lett. 22 (2022) 4589–4595.
[30] T.J. Park, J.H. Kim, J.H. Jang, U.K. Kim, S.Y. Lee, J. Lee, H.S. Jung, C.S. Hwang, Improved growth and electrical properties of atomic-layer-deposited metal-oxide film by discrete feeding method of metal precursor, Chem. Mater. 23 (2011) 1654–1658.
[31] H. Song, D. Shin, J.-e. Jeong, H. Park, D.-H. Ko, Growth behavior and film properties of titanium dioxide by plasma-enhanced atomic layer deposition with discrete feeding method, AIP Adv. 9 (2019).
[32] H.-N. Hung, C.-Y. Cheng, I.-C. Cheng, J.-J. Shyue, C.-C. Wang, F.-Y. Tsai, Enhancing electronic properties by suppressing nucleation delay for low-temperature processed atomic-layer-deposited amorphous zinc–tin-oxide thin films, Ceram. Int. 50 (9) (2024) 15085–15091.
[33] A.J. Lee, S. Lee, D.H. Han, Y. Kim, W. Jeon, Enhancing chemisorption efficiency and thin-film characteristics via a discrete feeding method in high-k dielectric

atomic layer deposition for preventing interfacial layer formation, J. Mater. Chem. C 11 (2023) 6894–6901.
[34] Y. Jang, S.M. Lee, D.H. Jung, J.H. Yum, E.S. Larsen, C.W. Bielawski, J. Oh, Improved dielectric properties of BeO thin films grown by plasma enhanced atomic layer deposition, Solid State Electron. 163 (2020) 107661.
[35] W.-H. Lee, W.-C. Kao, Y.-T. Yin, S.-H. Yi, K.-W. Huang, H.-C. Lin, M.-J. Chen, Sub-nanometer heating depth of atomic layer annealing, Appl. Surf. Sci. 525 (2020) 146615.
[36] S. Carniglia, J. Hove, Fabrication and properties of dense beryllium oxide, J. Nucl. Mater. 4 (1961) 165–176.
[37] D.S. Kwon, W. Jeon, D.G. Kim, T.K. Kim, H. Seo, J. Lim, C.S. Hwang, Improved properties of the atomic layer deposited Ru electrode for dynamic random-access memory capacitor using discrete feeding method, ACS Appl. Mater. Interfaces 13 (2021) 23915–23927.
[38] S.M. Lee, J.H. Yum, E.S. Larsen, S. Shervin, W. Wang, J.H. Ryou, C.W. Bielawski, W.C. Lee, S.K. Kim, J. Oh, Domain epitaxy of crystalline BeO films on GaN and ZnO substrates, J. Am. Ceram. Soc. 102 (2019) 3745–3752.
[39] S. Mustapha, M. Ndamitso, A. Abdulkareem, J. Tijani, D. Shuaib, A. Mohammed, A. Sumaila, Comparative study of crystallite size using Williamson-Hall and Debye-Scherrer plots for ZnO nanoparticles, Adv. Nat. Sci. Nanosci. Nanotechnol. 10 (2019) 045013.
[40] S. Fatimah, R. Ragadhita, D.F. Al Husaeni, A.B.D. Nandiyanto, How to calculate crystallite size from x-ray diffraction (XRD) using Scherrer method, ASEAN J.Sci Eng. 2 (2022) 65–76.
[41] H.-m. Kim, W.-B. Lee, H. Koo, S.-Y. Kim, J.-S. Park, Controlled 2D growth approach via atomic layer deposition for improved stability and performance in flexible SnO thin-film transistors, J. Mater. Chem. C 12 (23) (2024) 8390–8397.
[42] S.I. Park, B.C. Yang, J. Kim, J. Ko, G.M. Choi, J. An, J. Cho, Thermal conductivity of yttria-stabilized zirconia thin films grown by plasma-enhanced atomic layer deposition, J. Am. Ceram. Soc. 106 (2023) 5454–5463.
[43] J. Cho, J. Park, F.B. Prinz, J. An, Thermal conductivity of ultrathin BaTiO3 films grown by plasma-assisted atomic layer deposition, Scr. Mater. 154 (2018) 225–229.
[44] T. Nguyen, S. Lefrant, XPS study of SiO thin films and SiO-metal interfaces, J. Phys. Condens. Matter 1 (1989) 5197.
[45] Z. Liu, Y. Tang, N. Liao, P. Yang, Study on interfacial interaction between Si and ZnO, Ceram. Int. 45 (2019) 21894–21899.
[46] C. Wenger, M. Lukosius, G. Weidner, H.-J. Müssig, S. Pasko, C. Lohe, The role of the HfO2–TiN interface in capacitance–voltage nonlinearity of Metal-Insulator-Metal capacitors, Thin Solid Films 517 (2009) 6334–6336.
[47] H.L. Yang, H.-M. Kim, S. Kamimura, A. Eizawa, T. Teramoto, C. Dussarrat, O. Takashi, J.-S. Park, Boosted growth rate using discrete reactant feeding method and novel precursor of indium oxide by atomic layer deposition, Appl. Surf. Sci. 654 (2024) 159508.
[48] M. Nichols, W. Li, D. Pei, G. Antonelli, Q. Lin, S. Banna, Y. Nishi, J.L. Shohet, Measurement of bandgap energies in low-k organosilicates, J. Appl. Phys. 115 (2014).
[49] D.M. Fleetwood, Border traps and bias-temperature instabilities in MOS devices, Microelectron. Reliab. 80 (2018) 266–277.